


 Cite this: *RSC Adv.*, 2022, **12**, 16732

# Adsorption of gas molecules on buckled GaAs monolayer: a first-principles study

Rifat Shahriar, Orchi Hassan and Md. Kawsar Alam \*

The design of sensitive and selective gas sensors can be significantly simplified if materials that are intrinsically selective to target gas molecules can be identified. In recent years, monolayers consisting of group III–V elements have been identified as promising gas sensing materials. In this article, we investigate gas adsorption properties of buckled GaAs monolayer using first-principles calculations within the framework of density functional theory. We examine the adsorption energy, adsorption distance, charge transfer, and electron density difference to study the strength and nature of adsorption. We calculate the change in band structure, work function, conductivity, density of states, and optical reflectivity for analyzing its prospect as work function-based, chemiresistive, optical, and magnetic gas sensor applications. In this regard, we considered the adsorption of ten gas molecules, namely NH<sub>3</sub>, NO<sub>2</sub>, NO, CH<sub>4</sub>, H<sub>2</sub>, CO, SO<sub>2</sub>, HCN, H<sub>2</sub>S, and CO<sub>2</sub>, and noticed that GaAs monolayer is responsive to NO, NO<sub>2</sub>, NH<sub>3</sub>, and SO<sub>2</sub> only. Specifically, NH<sub>3</sub>, SO<sub>2</sub> and NO<sub>2</sub> chemisorb on the GaAs monolayer and change the work function by more than 5%. While both NO and NO<sub>2</sub> are found to be responsive in the far-infrared (FIR) range, NO shows better spin-splitting property and a significant change in conductivity. Moreover, the recovery time at room temperature for NO is observed to be in the sub-millisecond range suggesting selective and sensitive NO response in GaAs monolayer.

 Received 29th March 2022  
 Accepted 30th May 2022

DOI: 10.1039/d2ra02030k

[rsc.li/rsc-advances](http://rsc.li/rsc-advances)

## 1 Introduction

With the increased emission of toxic gas molecules due to the rapid progress of industrialization, the detection of gas molecules is critical. In this regard, the design and fabrication of stable, sensitive, and selective gas sensing devices that can detect molecules at a part per billion (ppb) concentration is crucial. Traditional MOS devices have high selectivity but do not have high sensitivity for detection at low concentrations.<sup>1</sup> To achieve high sensitivity, 2D materials with their high surface-to-volume ratio showed great promise facilitating sensing in concentration as low as 1 ppb.<sup>2,3</sup> However, 2D materials such as graphene-based chemiresistive sensors lack selectivity.<sup>4</sup> Plasmonic and photonic gas sensors are used to selectively detect and capture gas molecules to overcome this issue.<sup>5,6</sup> However, if materials are found that are intrinsically selective towards certain gas molecules, that is, adsorbs only certain molecules or has a distinct electronic or optical response, then the design of gas sensing devices can be much simpler without the need of complex devices. Thus, first-principles studies predicting the gas adsorbing behavior of emerging two-dimensional materials for identifying potential 2D materials have become a vital step in taking gas sensor research forward. 2D materials such as

graphene have been experimentally reported to be useful in the sensitive detection of gas molecules.<sup>7,8</sup> Single-atom doping of MoS<sub>2</sub> has been reported to increase sensitivity towards biomolecules such as dopamine.<sup>9</sup> Various 2D materials have been theoretically predicted to be excellent candidates for gas sensing application, such as, graphene,<sup>10–14</sup> Stanene,<sup>15,16</sup> MoS<sub>2</sub>,<sup>17</sup> SiC,<sup>18</sup> GeS,<sup>19</sup> GaN,<sup>20</sup> InN<sup>21</sup> *etc.* Monolayers consisting of group III–V elements have also been predicted to be excellent gas sensing materials in the literature.<sup>22–25</sup> For instance, hexagonal BAs is predicted to be a good candidate for SO<sub>2</sub> sensor,<sup>26</sup> whereas InN monolayer has shown strong SO<sub>2</sub> and NO<sub>2</sub> adsorption.<sup>27</sup> Recent reports on GaAs monolayer have demonstrated that it has high carrier mobility, tunable band gap, and strong second harmonic generation (SHG) response.<sup>28–30</sup> However, the adsorption of gas molecules on low buckled GaAs monolayer has not been investigated yet. The success of III–V monolayers in gas sensing and gas capturing combined with the excellent electronic and optical properties of GaAs monolayer has prompted us to study the adsorption of gas molecules on GaAs monolayer.

Therefore, in this work, we performed first-principles calculations to find out the adsorption property of ten gas molecules (NH<sub>3</sub>, NO<sub>2</sub>, NO, CH<sub>4</sub>, H<sub>2</sub>, CO, SO<sub>2</sub>, HCN, H<sub>2</sub>S, CO<sub>2</sub>) on GaAs monolayer. NO<sub>x</sub> and SO<sub>2</sub> are toxic gas molecules that are reported to cause respiratory problems, photochemical smog, and acid rain.<sup>31–36</sup> Other toxic gas molecules such as H<sub>2</sub>S, and NH<sub>3</sub> can cause burns in the skin, mouth, throat, and lungs and

Department of Electrical and Electronic Engineering, Bangladesh University of Engineering and Technology, Dhaka 1205, Bangladesh. E-mail: [kawsaralam@eee.buet.ac.bd](mailto:kawsaralam@eee.buet.ac.bd); [kawsar.alam@alumni.ubc.ca](mailto:kawsar.alam@alumni.ubc.ca)



can even be life-threatening.<sup>37–39</sup> On the other hand, detection of CO, HCN, CH<sub>4</sub>, and H<sub>2</sub> is critical due to the dangers of carbon monoxide poisoning,<sup>40,41</sup> inhibition of the consumption of oxygen by body tissues,<sup>42</sup> accidental explosion,<sup>43–46</sup> and coal mine accidents.<sup>47</sup>

Four adsorption sites have been considered for each gas, and adsorption energy has been calculated to determine the most energetically favorable configuration. The strength and nature of the adsorption have been elucidated by adsorption distance, Hirshfeld charge transfer, and electron density difference. The stability of GaAs monolayer upon gas adsorption has been examined by phonon dispersion calculations. The electronic structure of the gas analyte system was examined by partial density of states (PDOS) and band structure analysis. The prospect of the materials being used as a gas sensor has been investigated by calculating the work function, conductivity, reflectivity, magnetic moment, and recovery time of all the GaAs analyte systems. The next section explains the computational details and method.

## 2 Method and computational details

First-principles density function theory (DFT) has been used throughout this work. DFT calculations have been carried out using DMol<sup>3</sup> (ref. 48) and CASTEP<sup>49</sup> modules of Materials Studio. At first, a 3 × 3 supercell of GaAs monolayer was prepared by cleaving the bulk GaAs crystal, as shown in Fig. 1. A large vacuum slab of 21 Å was added to minimize spurious interaction with periodic images. The value of 21 Å is reported to be enough for accurate calculations of electronic and optical properties of GaAs monolayer.<sup>50</sup> Substrates can impact the properties of a two-dimensional material. Previous reports show that metallic states can appear on the interface states between the substrate material, and atomic layer janus MoSSe.<sup>51</sup> In gas or adatom adsorption, the presence of a substrate can enhance the adsorption energy and charge transfer between an adsorbent gas or dopant atom and the adsorbing material.<sup>52,53</sup> However, the experimental performance of 2D material based gas sensors with substrate has been successfully predicted by modelling the free standing monolayer in DFT calculation in past studies.<sup>9,54</sup> Hence, we used freestanding GaAs to model gas adsorption for less computational load.

The obtained GaAs monolayer was relaxed using the DMol<sup>3</sup> module until energy and force were converged to 1.0 × 10<sup>−7</sup> Ha and 1.0 × 10<sup>−4</sup> Ha per Å, respectively. The band structure, density of states, and Hirshfeld charge analyses of 3 × 3 supercell of the relaxed pristine GaAs monolayer were performed with DMol<sup>3</sup> module while the optical properties and phonon spectra were obtained using the CASTEP module. Monkhorst-Pack grid of 10 × 10 × 1 and 16 × 16 × 1 were used for geometry optimization and electronic structure calculation, respectively. Fermi level smearing was taken as 0.005 Ha. Double numerical polarized plus (DNP+) basis set was used with a global orbital cutoff of 5.0 Å. Generalized gradient approximation (GGA) with Perdew–Burke–Ernzerhof functional was used in all calculations. Hybrid Heyd, Scuseria, Ernzerhoff (HSE06) functional provides band gap values that are in

excellent agreement with the experimental values. However, in gas sensing, the change of band gap is more of interest than the absolute value of band gap. Hence, in accordance with the previous DFT studies on gas sensing, GGA-PBE functional was selected for computational efficiency.<sup>18,55</sup> For dispersion correction, taking van der Waals interactions into account, DFT-D dispersion correction method provided by Grimme was used. Gas molecules were subsequently added to the considered initial adsorption sites to determine the most stable site of adsorption. The four chosen initial adsorption sites: Ga (top of Ga atom), As (top of As atom), hollow (top of the center of hexagon), and bridge (top of Ga–As bonds), are shown in Fig. 1. Furthermore, as can be seen from Fig. 1, the Ga (As) protrusion is upwards (downwards). This can lead to non-identical adsorption on both sides. Hence, we added the gas molecules to both sides. A comparison between adsorption energies of the gas molecules on Ga protruded side and As protruded side is summarized in Table 1. After the adsorption, these structures were relaxed using the same parameters used in the structural relaxation of the pristine monolayer. Then the adsorption energy and the charge transfer of gas adsorbed systems were calculated as follows:<sup>56</sup>

$$E_{\text{ad}} = E(\text{gas} + \text{GaAs}) - E(\text{GaAs}) - E(\text{gas}) \quad (1)$$

$$\Delta\rho = \rho(\text{gas} + \text{GaAs}) - \rho(\text{GaAs}) - \rho(\text{gas}) \quad (2)$$

Here  $E_{\text{ad}}$ ,  $E(\text{gas})$ ,  $E(\text{gas} + \text{GaAs})$ , and  $E(\text{GaAs})$  represent adsorption energy, the energy of the isolated adsorbate gas molecule, gas adsorbed GaAs monolayer, and pristine GaAs monolayer, respectively. A negative value of  $E_{\text{ad}}$  denotes strong exothermic interaction and thermally stable adsorption. The larger the absolute value of  $E_{\text{ad}}$ , the stronger the interaction. Only the most energetically favorable configurations were considered for the subsequent analysis.  $\rho(\text{gas} + \text{GaAs})$ ,  $\rho(\text{GaAs})$ ,  $\rho(\text{gas})$  are the charge on gas adsorbed GaAs monolayer, pristine GaAs monolayer, and gas molecule, respectively. The calculated adsorption energy from eqn (1) is not a direct measure of experimental adsorption energy. Hence, zero point vibrational energy (ZPVE) was taken into account, and corrected adsorption energy,  $E'_{\text{ad}}$

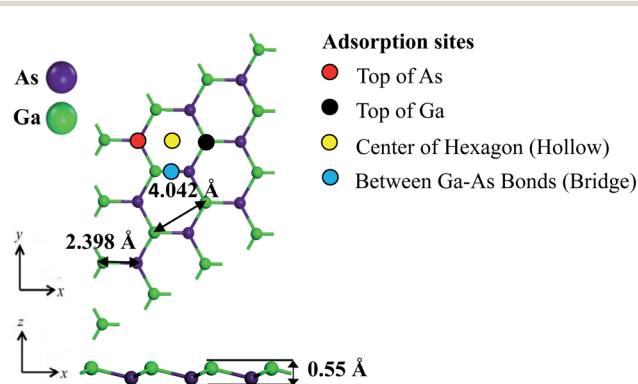


Fig. 1 Optimized structure of GaAs monolayer showing the lattice constant of 4.042 Å, bond length 2.398 Å, buckling height of 0.55 Å, and the four adsorption sites.



**Table 1** Comparison between adsorption energy on Ga protruded side vs. As protruded side

Gas	Ga protruded side	As protruded side
NH <sub>3</sub>	-0.88451	-0.59604
NO <sub>2</sub>	-1.28484	-1.48732
NO	-0.44763	-0.27312
H <sub>2</sub>	-0.10449	-0.10417
CO	-0.28088	-0.15979
CH <sub>4</sub>	-0.19513	-0.18613
SO <sub>2</sub>	-0.8167	-0.39242
HCN	-0.30572	-0.14357
H <sub>2</sub> S	-0.42689	-0.23032
CO <sub>2</sub>	-0.13274	-0.13543

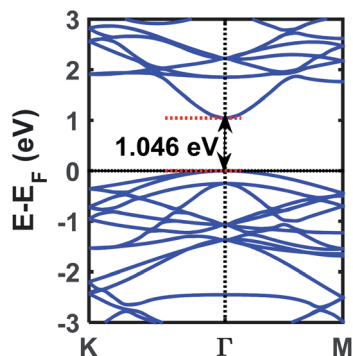
was also calculated according to the equation  $E'_{ad} = (E + ZPVE)_{gas+GaAs} - (E + ZPVE)_{gas} - (E + ZPVE)_{GaAs}$ . The dynamic stability of gas adsorption was also verified using phonon spectra calculations, and the supercell cutoff radius was selected to be 5 Å.

After verifying the stability of gas adsorption, the band structure and density of states calculation and the Hirshfeld charge analysis were performed on the gas adsorbed GaAs monolayers to determine the nature and mechanisms of gas adsorption. Finally, the gas sensing performance of GaAs monolayer was examined where, conductivity, reflectivity, magnetic moment, and work function were considered to be the sensing parameters.

## 3 Results and discussion

### 3.1 Benchmarking the simulation method and parameters

The electronic and structural properties were studied first to benchmark the simulation method and parameters and to study the change of electronic properties after gas adsorption. GaAs monolayer is found to be a low buckled monolayer with a bond length of 2.398 Å, lattice constant of 4.042 Å, and buckling height of 0.55 Å. The results are in agreement with previous theoretical studies.<sup>30,50,57</sup> The band gap of GaAs monolayer is calculated to be 1.046 eV from the GaAs monolayer

**Fig. 2** The band structure of pristine GaAs monolayer with a band gap of 1.046 eV.

band structure (shown in Fig. 2), which is also in agreement with previous studies performed at the PBE level of theory.<sup>30</sup> These results also serve as the reference for subsequent analyses on gas-adsorbed GaAs monolayer.

### 3.2 Adsorption configurations of gas molecules on GaAs monolayer

Geometry optimization was performed on all considered gas molecules and adsorbed configurations, and the corresponding adsorption energy was calculated. The most energetically favorable optimized structures that are considered for further analysis are shown in Fig. 3. As seen in Fig. 3, different gas molecules favor different adsorption sites, and the orientations of gas molecules are also disparate—some gas molecules get adsorbed with the molecules parallel to the GaAs monolayer surface. In contrast, other gas molecules get adsorbed with vertical or oblique orientation.

The shortest distance from the gas molecule to the GaAs surface ( $D$ ) is also observed to differ. The nature of bonding between the gas molecules and GaAs monolayer is influenced by this distance,  $D$  and it helps in understanding the nature of adsorption. The bonding was determined using the bond calculator tool of Materials Studio, which uses the criterion that  $D$  needs to be within the following range:

$$0.6 \times D_1 < D < 1.15 \times D_1, \quad (3)$$

where  $D_1 = R_{cov}(\text{Atom1}) + R_{cov}(\text{Atom2})$  and  $R_{cov}$  denotes the covalent radius of the atom.

The charge transfer and adsorption energy are also taken into account for determining the nature of adsorption. In general, adsorption energy of  $-0.5$  eV or less (greater in absolute value) is required for chemisorption.<sup>58–60</sup> The adsorption configurations and the nature of adsorption for the gas molecules are discussed in the following portion.

**3.2.1 NH<sub>3</sub>.** For NH<sub>3</sub> adsorption on GaAs monolayer, the adsorption energy was calculated to be  $-0.76$  eV, indicating highly energetically favorable adsorption. The preferred adsorption site was the top of the Ga atom on the Ga protruded side as can be seen from Fig. 3(a). NH<sub>3</sub> molecule forms a Ga–N bond with a bond length of 2.138 Å. The calculated Hirshfeld charge transfer is  $0.2433|e|$ . The Ga atom that bonded with the NH<sub>3</sub> molecule has a charge of  $0.274|e|$  on it, which can also be observed from the large charge depletion on the Ga atom that bonds with the NH<sub>3</sub> molecule, as can be seen in Fig. 4(a). Large adsorption energy combined with high charge transfer indicates that NH<sub>3</sub> molecule chemisorbs on GaAs monolayer.

**3.2.2 NO<sub>2</sub>.** In the case of NO<sub>2</sub> adsorption, the NO<sub>2</sub> molecule was observed to get adsorbed close to the top of the Ga atom of the As protruded side as seen in Fig. 3(b). In this case, oxygen atom of NO<sub>2</sub> was directly above the Ga atom of GaAs monolayer with the NO<sub>2</sub> molecule parallel to the GaAs monolayer. The Ga atom of GaAs monolayer formed a Ga–O bond with a bond length of 2.023 Å. The calculated adsorption energy was  $-1.46$  eV which indicates highly energetically favorable adsorption. A high charge transfer of  $0.2803|e|$  from GaAs to NO<sub>2</sub> was also observed. In Fig. 4(b), the high charge



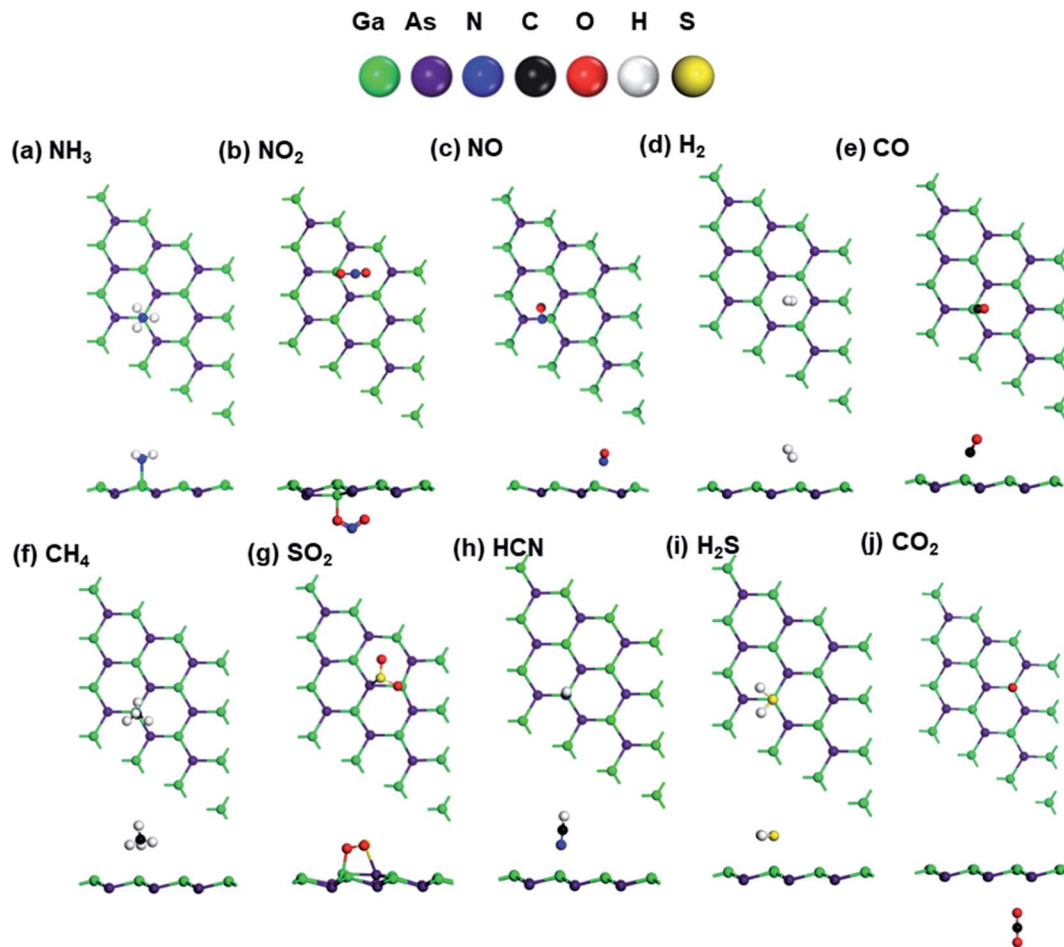


Fig. 3 Top and side view of the most energetically favorable adsorption configuration of the adsorbed molecules (a)  $\text{NH}_3$ , (b)  $\text{NO}_2$ , (c)  $\text{NO}$ , (d)  $\text{H}_2$ , (e)  $\text{CO}$ , (f)  $\text{CH}_4$ , (g)  $\text{SO}_2$ , (h)  $\text{HCN}$ , (i)  $\text{H}_2\text{S}$ , and (j)  $\text{CO}_2$  molecules on the GaAs monolayer. The balls of the colors green, violet, blue, red, black, yellow, and white represent Ga, As, N, O, C, S, and H.

accumulation on  $\text{NO}_2$  molecule and depletion on GaAs can be seen, which confirms the high charge transfer. The low adsorption distance, high charge transfer, and adsorption energy are indicative of chemisorption.

**3.2.3 NO.** The most stable adsorption site for the  $\text{NO}$  molecule was observed to be the bridge site of the Ga protruded side, although the  $\text{NO}$  molecule was not in the exact center of the Ga–As bond. Instead, the  $\text{NO}$  molecule was closer to the top of the Ga atom than the top of the As atom, as shown in Fig. 3(c). Adsorption energy was found to be  $-0.39$  eV, and the calculated adsorption distance was  $2.188$  Å. No bond formation between the  $\text{NO}$  molecule and GaAs monolayer was observed. However, a moderately high charge transfer of  $0.18|e|$  was noted. The charge accumulation on the N atom of  $\text{NO}$  molecule and charge depletion on GaAs monolayer can be seen in Fig. 4(c). Nonetheless, an adsorption energy less than  $|0.5|$  eV with a large adsorption distance is indicative of physisorption. Hence, it can be concluded that  $\text{NO}$  molecule is physisorbed on GaAs monolayer.

**3.2.4  $\text{H}_2$ .** From Fig. 3(d), it can be seen that the most stable site for the  $\text{H}_2$  molecule on GaAs monolayer was the hollow site of the Ga protruded side. Adsorption energy was  $-0.07$  eV. Very

low adsorption energy is indicative of weak adsorption. Charge transfer was also low:  $0.045|e|$ , when  $\text{H}_2$  molecule was adsorbed on GaAs monolayer. The electron density difference plot in Fig. 4(d) shows no perceptible charge accumulation or depletion. The adsorption distance was  $3.155$  Å. The low adsorption energy, high adsorption distance, and negligible charge transfer confirm the physisorption of  $\text{H}_2$  molecules on GaAs monolayer.

**3.2.5 CO.**  $\text{CO}$  molecule was adsorbed on top of the Ga atom with the carbon atom close to the Ga atom of the Ga protruded side, as can be seen in Fig. 3(e). Adsorption energy was  $-0.24$  eV. A moderate Hirshfeld charge transfer of  $0.0081|e|$  was calculated. The charge transfer can also be observed from the charge depletion on GaAs monolayer surface and charge accumulation on the  $\text{CO}$  molecule, as shown in Fig. 4(e). The adsorption distance was large— $2.147$  Å, and no bond formation was detected. Because of the low adsorption energy and long adsorption distance, we can conclude the  $\text{CO}$  physisorbed on GaAs monolayer.

**3.2.6  $\text{CH}_4$ .** In the case of  $\text{CH}_4$  adsorption, as shown in Fig. 3(f), the most stable adsorption site was the Ga site of the Ga protruded side. Adsorption energy was  $-0.21$  eV. Very low adsorption energy is indicative of very weak adsorption.



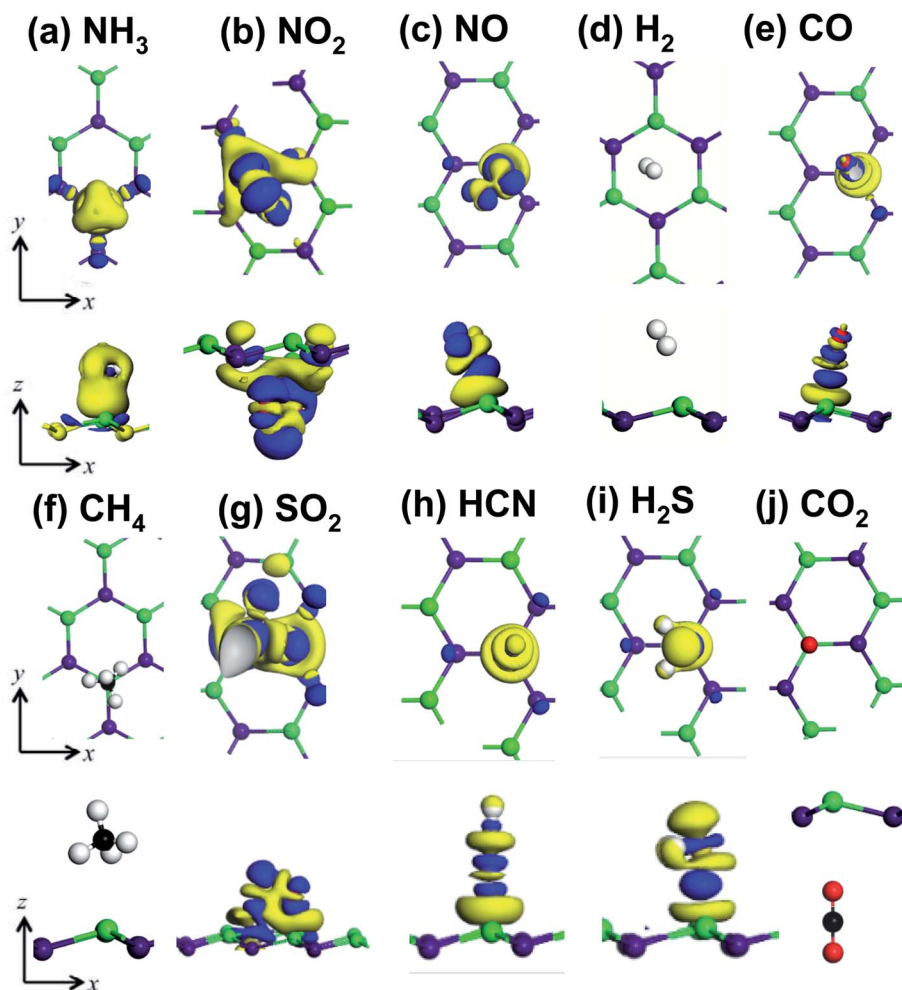


Fig. 4 Electron density difference plots of (a)  $\text{NH}_3$ , (b)  $\text{NO}_2$ , (c)  $\text{NO}$ , (d)  $\text{H}_2$ , (e)  $\text{CO}$ , (f)  $\text{CH}_4$ , (g)  $\text{SO}_2$ , (h)  $\text{HCN}$ , (i)  $\text{H}_2\text{S}$ , and (j)  $\text{CO}_2$  adsorbed GaAs monolayer. Here the blue (yellow) color denotes electron accumulation (depletion). Isovalue is 0.01 electrons per  $\text{\AA}^3$ .

Adsorption distance was 3.006 Å while the charge transfer was  $0.09|e|$ . The low charge transfer is also evident from Fig. 4(f) where no charge accumulation or depletion can be seen. A high adsorption distance means that only weak van der Waals attraction existed between the  $\text{CH}_4$  molecule and GaAs monolayer. These results indicate that although GaAs monolayer might not be appropriate for  $\text{CH}_4$  adsorption, GaAs monolayer was unaffected by  $\text{CH}_4$  molecule, which means that  $\text{CH}_4$  molecule might not inhibit the sensing performance in the case of other molecules.

**3.2.7  $\text{SO}_2$ .** The most energetically preferable site of adsorption for  $\text{SO}_2$  was observed to be the bridge site of the Ga protruded side. The S atom of  $\text{SO}_2$  bonded with the As atom while the O atom bonded with the Ga atom as can be seen from Fig. 3(g). The shortest distance between the  $\text{SO}_2$  atom and GaAs monolayer surface was 1.954 Å. The adsorption energy was calculated to be  $-0.78$  eV. Hirshfeld charge transfer indicates that  $0.2643|e|$  transferred from GaAs monolayer to the  $\text{SO}_2$  monolayer. A large amount of charge piling up between  $\text{SO}_2$  and GaAs monolayer is presented in Fig. 4(g). The large charge transfer along with the high adsorption energy and low

adsorption distance indicates that  $\text{SO}_2$  chemisorbed on GaAs monolayer.

**3.2.8  $\text{HCN}$ .** The most stable site for  $\text{HCN}$  adsorption on GaAs monolayer, was the Ga site of the Ga protruded side as can be seen in Fig. 3(h). The  $\text{HCN}$  molecule was vertical and the distance between the N atom and Ga atom was 2.313 Å. The calculated adsorption energy was  $-0.25$  eV and the Hirshfeld charge transfer was  $0.1643|e|$ . A moderate amount of charge depletion was observed between the N atom of  $\text{HCN}$  and GaAs monolayer which can be observed in Fig. 4(h). Charge accumulation was observed between the C atom and N atom of the  $\text{HCN}$  molecule. Since the absolute value of adsorption energy was lower than 0.5 eV and the adsorption distance was high, it can be concluded that the  $\text{HCN}$  molecule physisorbed on the GaAs monolayer.

**3.2.9  $\text{H}_2\text{S}$ .** The most stable site for  $\text{H}_2\text{S}$  molecule was the Ga site of the Ga protruded side. The  $\text{H}_2\text{S}$  molecule was parallel to the GaAs monolayer surface with the S atom on top of the Ga atom as presented in Fig. 3(i). The distance between the Ga atom and the S atom on top of the Ga atom was 2.646 Å. The calculated adsorption energy was  $-0.34$  eV. The Hirshfeld



charge transfer was calculated to be  $0.1897|e|$ . Charge accumulation on the S atom and depletion on the Ga atom can be seen in Fig. 4(i). The large adsorption distance and low adsorption energy suggest that H<sub>2</sub>S molecule physisorbed on the GaAs monolayer.

**3.2.10 CO<sub>2</sub>.** The CO<sub>2</sub> molecule was adsorbed on the Ga site of the As protruded side with the CO<sub>2</sub> molecule vertical to the GaAs monolayer as can be seen in Fig. 3(j). The calculated adsorption energy was very low  $-0.1211$  eV. The adsorption distance between the CO<sub>2</sub> molecule and GaAs monolayer was 3.413 Å. Furthermore, the Hirshfeld charge transfer between the CO<sub>2</sub> molecule and GaAs monolayer was  $0.0081|e|$ . No charge piling between the CO<sub>2</sub> molecule and GaAs monolayer was observed as shown in Fig. 4(j). The low adsorption energy, high adsorption distance, and low charge transfer indicate that CO<sub>2</sub> molecule physisorbed on the GaAs monolayer.

The difference between the GaAs—analyte systems, the adsorption energy ( $E_{ad}$ ), adsorption distance ( $D$ ), and Hirshfeld charge transfer ( $Q$ ) are summarized in Table 2. As can be seen

**Table 2** Adsorption energy ( $E_{ad}$ ), ZPVE corrected adsorption energy ( $E'_{ad}$ ), adsorption distance ( $D$ ), and Hirshfeld charge transfer ( $Q$ ) of the most energetically favorable gas adsorbed structures. A negative value of  $Q$  indicates charge transfer from GaAs to the gas molecule

Gas molecule	$E_{ad}$ (eV)	$E'_{ad}$ (eV)	$Q$ ( $ e $ )	$D$ (Å)	Type of adsorption
NH <sub>3</sub>	-0.8845	-0.7563	0.2433	2.138	Chemisorption
NO <sub>2</sub>	-1.4874	-1.4643	0.2803	2.023	Chemisorption
NO	-0.4476	-0.3889	-0.18	2.188	Physisorption
H <sub>2</sub>	-0.1044	-0.0741	0.045	3.155	Physisorption
CO	-0.2808	-0.2383	0.11	2.147	Physisorption
CH <sub>4</sub>	-0.1951	-0.2091	-0.09	3.006	Physisorption
SO <sub>2</sub>	-0.8167	-0.7843	-0.2643	1.954	Chemisorption
HCN	-0.3057	-0.2527	0.1643	2.313	Physisorption
H <sub>2</sub> S	-0.4269	-0.3421	0.1897	2.646	Physisorption
CO <sub>2</sub>	-0.1354	-0.1211	0.0081	3.413	Physisorption

from Table 2, NH<sub>3</sub>, NO<sub>2</sub>, and SO<sub>2</sub> are chemisorbed on GaAs monolayer while the other gas molecules are physisorbed.

### 3.3 Stability of the GaAs-analyte systems

Before studying the electronic and optical properties of the various gas adsorbed systems, the phonon spectra of the gas adsorbed systems were calculated to verify the dynamic stability of the gas adsorption. No imaginary frequency was observed in the case of the adsorption of any of the gas molecules except CH<sub>4</sub> (Fig. 5(f)). Hence, CH<sub>4</sub> adsorption was not considered in any of the subsequent calculations.

### 3.4 The electronic structure of GaAs-analyte systems

The presence of gas molecules is expected to alter the electronic structures of GaAs monolayer. Hence, the orbital projected density of states and band structures were calculated. In Fig. 6 the band structures of all the gas adsorbed systems are presented. It can be seen from Fig. 6(b and e) that the effect of NH<sub>3</sub> and H<sub>2</sub> on the electronic properties of GaAs monolayer is negligible. The observed change in band gap was very small.

To understand the contribution of gas molecules in the electronic structure of the GaAs analyte systems, the projected density of states of the gas adsorbed structures was calculated. The N and H atoms of NH<sub>3</sub> or H<sub>2</sub> molecules have negligible contributions to the density of states, as seen in Fig. 7(a and d). However, when CO was adsorbed on the GaAs monolayer, a sizable change of 0.12 eV in the band gap was observed which can be seen in Fig. 6(f). Strong hybridization of p orbitals in the carbon atom, oxygen atom, and Ga atoms is observed at the 1.7–2 eV range, as can be seen in Fig. 7(e). This hybridization might have caused the conduction band to shift, which could have led to the change in band gap.

Strong hybridization also occurred when NO was adsorbed on GaAs. In this case, the hybridization occurred between p orbitals of N and O atoms. NO adsorption also gave rise to new

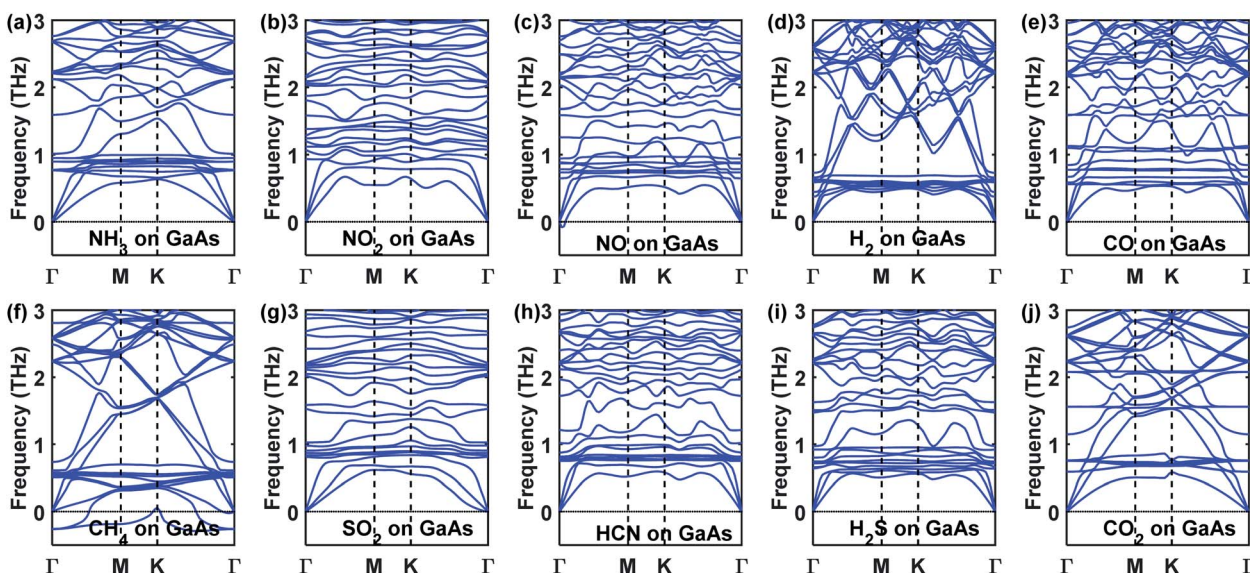


**Fig. 5** Phonon dispersion curves of (a) NH<sub>3</sub>, (b) NO<sub>2</sub>, (c) NO, (d) H<sub>2</sub>, (e) CO, (f) CH<sub>4</sub>, (g) SO<sub>2</sub>, (h) HCN, (i) H<sub>2</sub>S, and (j) CO<sub>2</sub> adsorbed GaAs monolayer.



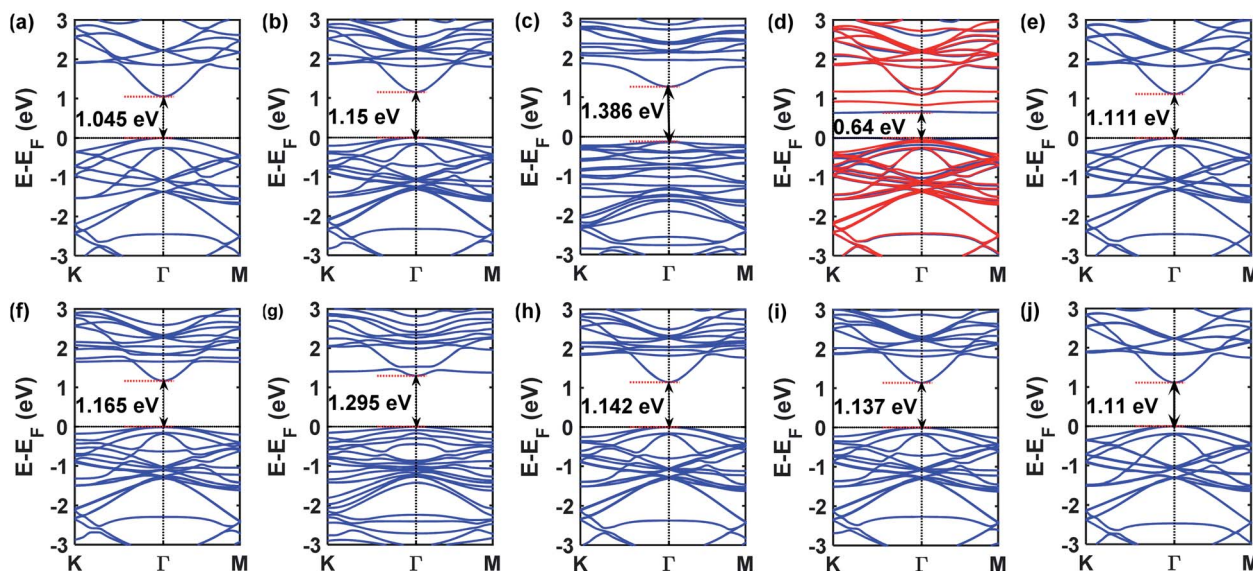


Fig. 6 The band structures of (a) pristine, and (b)  $\text{NH}_3$ , (c)  $\text{NO}_2$ , (d)  $\text{NO}$ , (e)  $\text{H}_2$ , (f)  $\text{CO}$ , (g)  $\text{SO}_2$ , (h)  $\text{HCN}$ , (i)  $\text{H}_2\text{S}$ , and (j)  $\text{CO}_2$  adsorbed GaAs monolayer. The blue (red) color indicates up (down) spin.  $\text{NO}$  adsorption substantially decreases the band gap to 0.64 eV, while other gas adsorbed structures have a band gap reasonably similar to the pristine band gap of 1.046 eV.

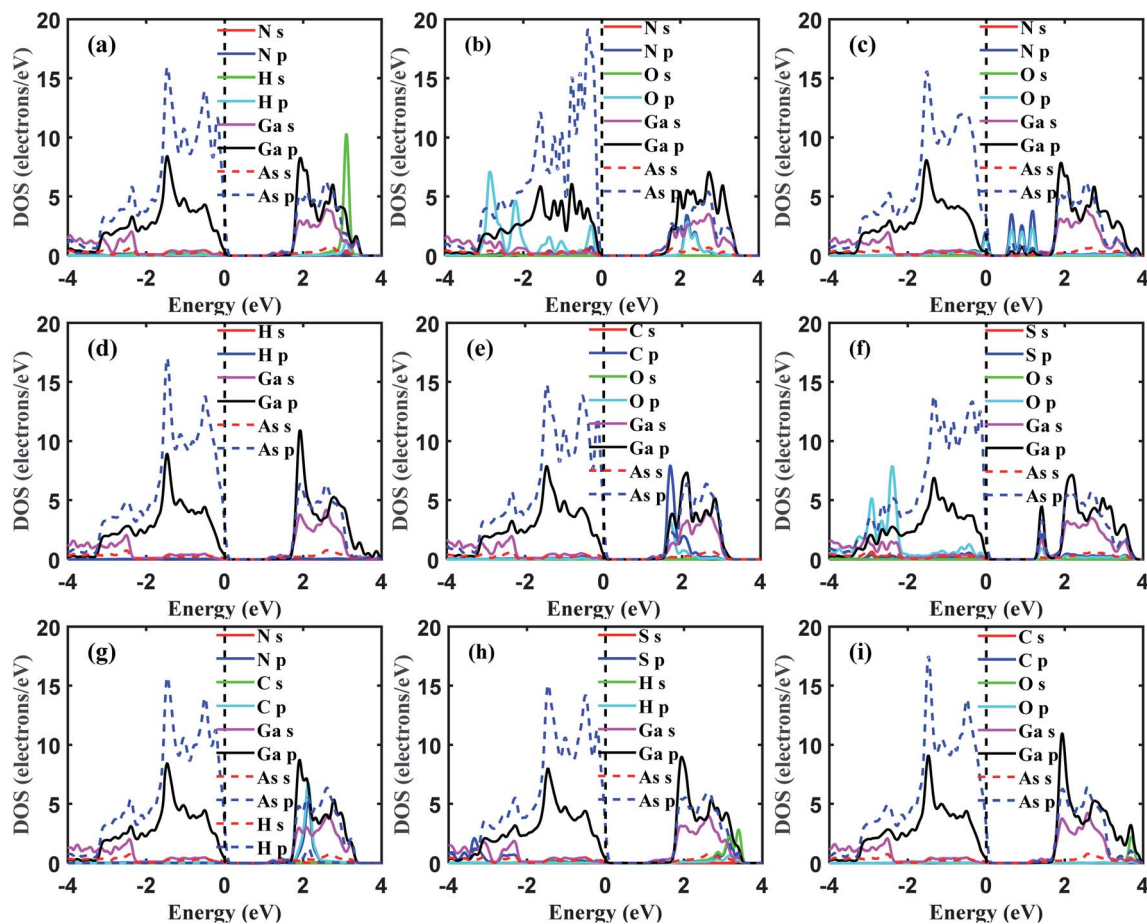


Fig. 7 The orbital projected density of states of (a)  $\text{NH}_3$ , (b)  $\text{NO}_2$ , (c)  $\text{NO}$ , (d)  $\text{H}_2$ , (e)  $\text{CO}$ , (f)  $\text{SO}_2$ , (g)  $\text{HCN}$ , (h)  $\text{H}_2\text{S}$ , and (i)  $\text{CO}_2$  adsorbed GaAs monolayer. The blue (red) color indicates up (down) spin.  $\text{NO}$  adsorption substantially decreases the band gap to 0.64 eV, while other gas adsorbed structures have a band gap reasonably similar to the pristine band gap of 1.046 eV.



states, as seen in Fig. 7(c). Because the new states arrived at the 0.5 to 1.5 eV region, the band gap decreased the most to 0.64 eV when NO was adsorbed, as can be seen in Fig. 6(d). Like NO adsorption, new states also appear when NO<sub>2</sub> gets adsorbed on the GaAs monolayer. Furthermore, strong hybridization between the orbitals of NO and GaAs was observed. In Fig. 7(b), it can be seen that p orbitals of N and O atoms hybridize with s and p orbitals of Ga and As around the 2 to 4 eV range. Furthermore, p orbitals of oxygen atoms hybridize with p orbitals of As and Ga atoms around -2 to -3 eV. Additionally, the orbital contribution from As atoms is higher than other gas adsorbed structures around 0 eV to -1 eV. So, the total density of states gets altered in the aforementioned ranges. The conduction band gets pushed upwards due to the interaction with NO<sub>2</sub> molecules and consequently the band gap increases by 0.34 eV. SO<sub>2</sub> adsorption altered the electronic structure of GaAs monolayer and increased the band gap to 1.295 eV as can be seen in Fig. 6(g). Strong hybridization between the p orbitals of Ga, O, and S atoms was observed in the 1.5 eV to 2 eV range in the conduction band. Furthermore, like NO<sub>2</sub> adsorption, SO<sub>2</sub> adsorption alters the density of states in the -2 to -4 eV range in the valence band. The p orbitals of O atom were observed to hybridize with p orbitals of Ga and As atoms (Fig. 7(f)). Hence two extra states were observed in the band structure in the -2 to -3 eV range as can be seen in Fig. 6(g). On the contrary, H<sub>2</sub>S adsorption did not alter the electronic structure of the GaAs monolayer. However, weak hybridization between the S and Ga atoms can be observed in the -2 to -4 eV range in the valence band as can be seen in Fig. 7(h). The band gap change was small (~0.09 eV). On the other hand, HCN adsorption modified the electronic structure of GaAs monolayer. As can be seen in Fig. 7(g), the p orbitals of the C atom in HCN molecule hybridized strongly with the p orbitals of the Ga atom in the 1.8 eV to 2.2 eV range in the conduction band. HCN adsorption resulted in a change of 0.097 eV as can be seen in Fig. 6(h). CO<sub>2</sub> adsorption did not alter the electronic structure of the GaAs monolayer much and the change in band gap was very small eV (~0.07 eV) as can be seen in Fig. 6(j).

### 3.5 Gas sensing performance of GaAs monolayer

In this section, we discuss the gas sensing possibilities utilizing different properties of GaAs monolayer. Different properties can be utilized for sensing, such as work function, band gap change, optical response, and magnetic moment.<sup>61–65</sup> We discuss each of them based on three main criteria: sensitivity, selectivity, and recovery time.

**3.5.1 The prospect of GaAs monolayer in work function-based sensor.** The work function ( $\Phi$ ) is an important property for optoelectronic devices. Furthermore, the work function of GaAs monolayer will dictate its Schottky barrier height with various metal electrodes and graphene electrodes. The work function of the pristine GaAs monolayer was calculated to be 5.143 eV. The work function of the gas adsorbed structures was then calculated. The work functions of the gas adsorbed GaAs monolayer are shown in Table 3. In Table 3,  $\Delta\Phi$  is defined as the difference between the work function of the gas adsorbed

**Table 3** The work functions of the gas adsorbed GaAs monolayer. GaAs monolayer has a sensitivity greater than 5% towards NH<sub>3</sub> and NO<sub>2</sub>

Adsorbed gas	$\Phi$ (eV)	$\Delta\Phi$ (eV)	$S$ (%)
NH <sub>3</sub>	4.842	-0.301	5.85
NO <sub>2</sub>	5.522	0.379	7.37
NO	5.196	0.053	1.03
H <sub>2</sub>	5.196	0.053	1.03
CO	5.196	0.053	1.03
SO <sub>2</sub>	5.415	0.272	5.29
HCN	4.789	-0.354	6.88
H <sub>2</sub> S	5.034	-0.109	2.12
CO <sub>2</sub>	5.007	0.136	2.64

structure and pristine GaAs, *i.e.*,  $\Delta\Phi = \Phi_{\text{GaAs+gas}} - \Phi_{\text{GaAs}}$ . The sensitivity,  $S$ , is defined as  $S = |\Delta\Phi/\Phi_{\text{GaAs}}| \times 100$ .

The work functions of NO, CO, and H<sub>2</sub> adsorbed GaAs monolayer was calculated to be 5.196 eV. The change in work function is not large in any of these cases. On the contrary, the work function of the NH<sub>3</sub>, NO<sub>2</sub>, SO<sub>2</sub>, and HCN adsorbed GaAs monolayer were 4.842 eV, 5.522 eV, 5.42 eV, and 4.789 eV, respectively. The calculated sensitivity was greater than 5% for all these cases. Hence, GaAs monolayer could be a sensitive material for NH<sub>3</sub>, NO<sub>2</sub>, SO<sub>2</sub>, and HCN detection in work-function based sensors.

**3.5.2 The prospect of GaAs monolayer in chemiresistive sensors.** The conductivity was calculated using the relation,<sup>66,67</sup>  $\sigma = A \exp\left(-\frac{E_g}{2k_B T}\right)$ . Here,  $A$  is a proportionality constant,  $E_g$  is the band gap of the pristine or gas adsorbed structure,  $k_B$  is the Boltzmann constant, and  $T$  is the temperature. The change of conductivity can thus be used to define sensitivity and can be expressed as

$$\frac{\delta\sigma}{\sigma} = \frac{\exp\left(-\frac{E_g(\text{GaAs} + \text{gas})}{2k_B T}\right) - \exp\left(-\frac{E_g(\text{GaAs})}{2k_B T}\right)}{\exp\left(-\frac{E_g(\text{GaAs})}{2k_B T}\right)} \quad (4)$$

The calculated sensitivity is shown in Table 4.

Since NO adsorbed GaAs monolayer has the greatest change in band gap, which is, 0.405 eV, the sensitivity of GaAs monolayer is the highest towards NO, which is  $2.54 \times 10^3$ . The band gap change is less than 0.34 eV, and the sensitivity is less than 1 in the case of all other molecules. Hence, GaAs could be used in chemiresistive sensors for selective detection of NO.

**3.5.3 The prospect of GaAs monolayer in optical gas sensors.** Optical gas sensors have gained popularity recently.<sup>68–70</sup> The change of optical properties such as absorption coefficient, reflectivity, dielectric function in the presence of gas molecules could be used for selective gas sensing. The benefit of optical gas sensors is that by tuning the sensor to different frequencies, the same material could be used for selective detection of different molecules. The reflectivity of GaAs monolayer was calculated before and after





Table 4 The sensitivity of GaAs monolayer towards different gas molecules

Gas molecule	Sensitivity
NH <sub>3</sub>	0.86
NO <sub>2</sub>	0.99
NO	$2.54 \times 10^3$
H <sub>2</sub>	0.71
CO	0.90
SO <sub>2</sub>	0.99
HCN	0.84
H <sub>2</sub> S	0.83
CO <sub>2</sub>	0.698

the gas adsorption of the considered molecules. The variation of reflectivity with respect to photon energy is presented in Fig. 8, where the incident light is perpendicular to the monolayer. The reflectivity of GaAs monolayer was sensitive towards NO and NO<sub>2</sub> molecules in the far-infrared (FIR) range as can be seen in Fig. 8.

The reflectivity of GaAs monolayer was calculated to be 0.1 in the 0 to 1 eV range, whereas the reflectivity of NO and NO<sub>2</sub> adsorbed GaAs monolayer were much higher, ranging from 0.4 to 0.12 in the 0 to 0.5 eV range. The reflectivity of NO and NO<sub>2</sub> adsorbed GaAs monolayers are distinct from each other too, which means that they can be distinctly detected. Furthermore, the reflectivity of NO and NO<sub>2</sub> adsorbed monolayers were less than the pristine monolayer in the visible range. At 2 eV, the reflectivity of the pristine monolayer was approximately 0.16, whereas the reflectivity of NO and NO<sub>2</sub> adsorbed GaAs monolayer was 0.13 and 0.14 respectively. These results indicate that GaAs monolayer could work as a selective and sensitive gas sensor in the visible range too.

**3.5.4 The prospect of GaAs monolayer in magnetic gas sensors.** Magnetic gas sensors have gained popularity in recent times due to their safety and lack of electrical contacts.<sup>71–73</sup> Hence, the prospect of GaAs monolayer as a magnetic gas sensor has been explored. Spin-polarized DFT calculations were

performed to analyze the magnetic moment of the gas adsorbed systems. It was found that magnetic moment was induced on GaAs monolayer when NO molecule was adsorbed on it. From the band structure plot in Fig. 6(e), it can be seen that magnetization occurred, which is indicated by the split of up spin and down spin conduction bands. The induced magnetism was further confirmed by the asymmetry in the up spin and down spin density of states as shown in Fig. 9(a). The induced magnetic moment was 1.02  $\mu_B$ . The spin density isosurface shown in Fig. 9(b) also confirms the induced magnetism. It can be seen that the magnetic moment is induced in the arsenic atoms adjacent to the adsorption site. It is to be noted that the magnetic moment is only induced when NO molecule is adsorbed on the GaAs monolayer surface. In all other cases, the GaAs—analyte system is non-magnetic. This distinct behavior towards NO molecule indicates that GaAs monolayer could be used as a magnetic gas sensor. The selectivity may be better than the previously reported cases where the magnetic moment was induced by multiple gas molecules.<sup>20,74</sup>

**3.5.5 Recovery time.** Recovery time is defined as the time required for an adsorbed gas molecule to spontaneously desorb from the adsorption surface. It is a crucial parameter that indicates the reusability of a gas sensor. The recovery time was calculated using the van't Hoff-Arrhenius equation,<sup>75</sup>

$$\tau = \nu_0^{-1} \exp\left(-\frac{E_{ad}}{k_B T}\right),$$

where  $\nu_0$  is the attempt frequency.

Previous reports determined the attempt frequency of NO<sub>2</sub> to be  $10^{12} \text{ s}^{-1}$ .<sup>76</sup> According to previous works, it is reasonable to assume the same attempt frequency for other gas molecules.<sup>18,77,78</sup> The considered temperature was 300 K. The recovery times at temperatures 300–600 K are summarized in Table 5.

The room temperature recovery time was calculated to be less than a millisecond for all of the gas adsorption cases except NH<sub>3</sub> and NO<sub>2</sub>. However, in high temperatures such as 400 K, the recovery time for NH<sub>3</sub> is less than a second. At 450 K, the recovery time for NO<sub>2</sub> is approximately 4.6 hours, which is reasonable.<sup>18,66</sup> At 500 K, the recovery time for NO<sub>2</sub> gets down to 615.32 seconds, which is a rapid recovery time.<sup>79</sup> Based on these

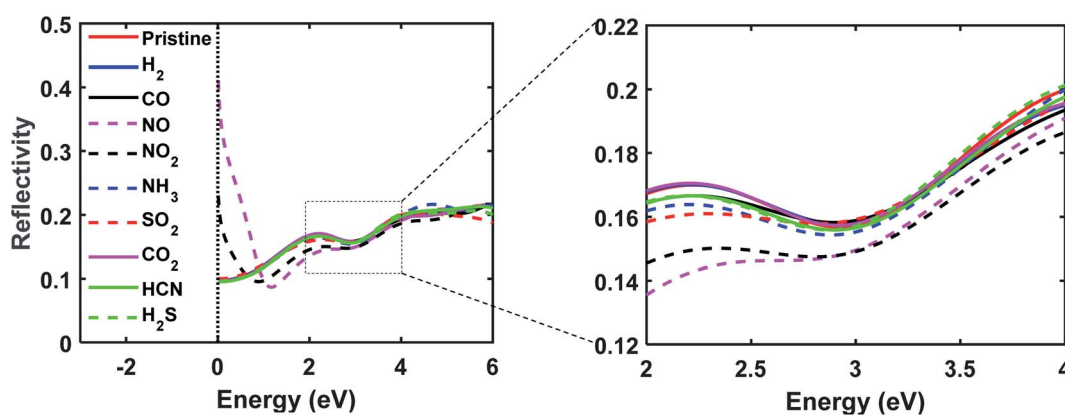


Fig. 8 The reflectivity of pristine and gas adsorbed GaAs monolayer. The reflectivity of NO and NO<sub>2</sub> adsorbed monolayers are higher than the pristine and other gas adsorbed monolayers in the 0–1 eV range. In the 4–6 eV range, the reflectivity curves are on top of each other, indicating that the value of reflectivity is the same for all structures in this range.



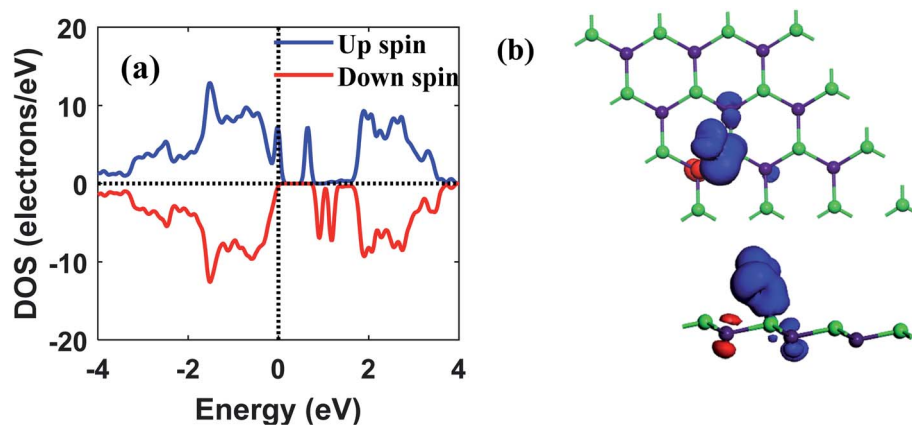


Fig. 9 (a) Spin resolved density of states in NO adsorbed GaAs monolayer; (b) the isosurface of showing spin density in NO adsorbed GaAs monolayer. Blue color represents up spin and red represents down spin. Isovalue is 0.005e per Angstrom<sup>3</sup>.

Table 5 The recovery time after gas adsorption for 300–600 K

Gas molecule	Recovery time (s) at 300 K	Recovery time (s) at 400 K	Recovery time (s) at 500 K	Recovery time (s) at 600 K
NH <sub>3</sub>	5.38	0.0035	$4.35 \times 10^{-5}$	$2.32 \times 10^{-6}$
NO <sub>2</sub>	$4.45 \times 10^{12}$	$3.07 \times 10^6$	615.52	2.11
NO	$3.52 \times 10^{-6}$	$8.13 \times 10^{-8}$	$8.471 \times 10^{-9}$	$1.88 \times 10^{-9}$
H <sub>2</sub>	$1.77 \times 10^{-11}$	$8.62 \times 10^{-12}$	$5.601 \times 10^{-12}$	$4.20 \times 10^{-12}$
CO	$1.03 \times 10^{-8}$	$1.02 \times 10^{-9}$	$2.55 \times 10^{-10}$	$1.01 \times 10^{-10}$
SO <sub>2</sub>	15.93	0.008	$8.34 \times 10^{-5}$	$3.99 \times 10^{-6}$
HCN	$1.79 \times 10^{-8}$	$1.55 \times 10^{-9}$	$3.57 \times 10^{-10}$	$1.34 \times 10^{-10}$
H <sub>2</sub> S	$5.74 \times 10^{-7}$	$2.08 \times 10^{-8}$	$2.85 \times 10^{-9}$	$7.57 \times 10^{-10}$
CO <sub>2</sub>	$1.09 \times 10^{-10}$	$3.38 \times 10^{-11}$	$1.67 \times 10^{-11}$	$1.05 \times 10^{-11}$

results, it can be concluded that GaAs monolayer could be a suitable candidate for reusable gas sensors.

**3.5.6 Diffusion analysis.** Gas diffusion on the adsorbent surface is an important factor in gas sensor performance.<sup>80,81</sup> Hence we calculated the diffusion of gas molecules on GaAs

monolayer. We calculated the diffusion using the transition state search algorithm of DMol<sup>3</sup> which performs a Linear Synchronous Transit (LST), followed by repeated conjugate gradient minimizations and Quadratic Synchronous Transit (QST) maximizations until a transition state has been located.

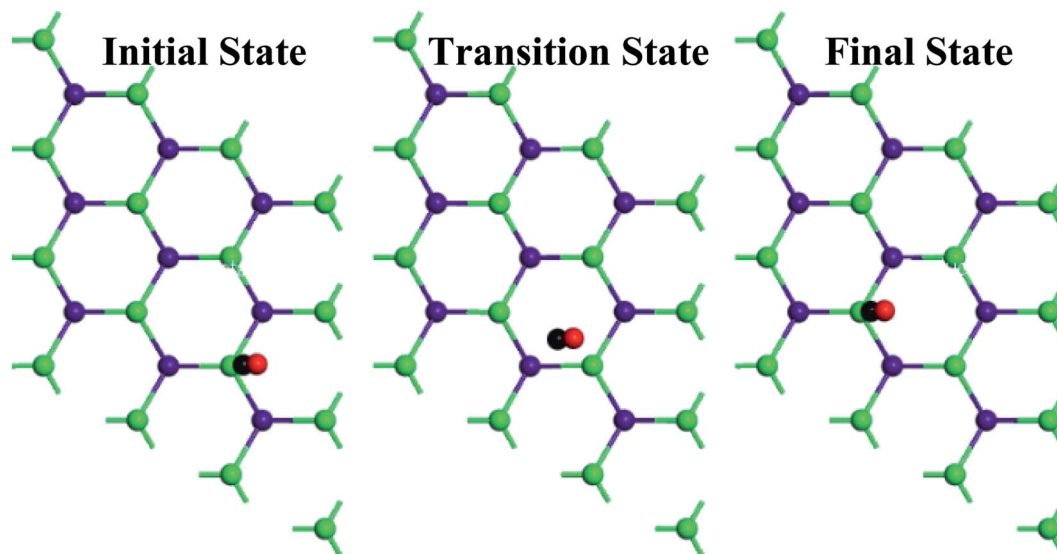


Fig. 10 Initial, transition, and final state for CO diffusion on GaAs monolayer.



Table 6 Diffusion barrier for the considered gas molecules

Gas	$E_{\text{bar}}$ (eV)
NH <sub>3</sub>	0.67
NO <sub>2</sub>	2.35
NO	0.33
H <sub>2</sub>	0.08
CO	0.25
CH <sub>4</sub>	0.12
SO <sub>2</sub>	0.67
HCN	0.24
H <sub>2</sub> S	0.27
CO <sub>2</sub>	0.08

To determine the diffusion barrier ( $E_{\text{bar}}$ ), we set an initial structure (which is the relaxed structure in our study), and an equivalent structure where the gas molecule is adsorbed on a neighboring equivalent site as demonstrated in Fig. 10 for CO as an example. The transition state search algorithm then generated the diffusion pathway, transition state, and barrier energy. The diffusion barriers are summarized in Table 6.

As can be seen in Table 6, H<sub>2</sub> and CO<sub>2</sub> can diffuse easily on the GaAs surface. The rest of the gas molecules have a higher diffusion barrier. However, the calculated diffusion barriers are comparable to the diffusion barriers of various gas molecules on TiO<sub>2</sub> nanoparticles.<sup>82</sup>

## 4 Conclusion

The prospect of buckled GaAs monolayer as a gas-sensing 2D material was systematically investigated using density functional theory. It was found that NH<sub>3</sub>, SO<sub>2</sub>, and NO<sub>2</sub> molecules chemisorb while NO, CO, H<sub>2</sub>, HCN, CO<sub>2</sub>, and H<sub>2</sub>S molecules physisorb on the GaAs monolayer. Our calculations show that NH<sub>3</sub> and HCN adsorption decreases the work function by 5.85% and 6.88%, while NO<sub>2</sub> and SO<sub>2</sub> adsorption increases the work function by 7.37% and 5.29% respectively. The adsorption of other gas molecules was observed to have minimal impact on the work function. It was also observed that NO adsorption decreases the band gap from 1.046 eV to 0.64 eV while the other gas molecules cause only very small changes. The calculated sensitivity of  $2.54 \times 10^3$  towards NO molecule suggests that GaAs monolayer could be a promising material for chemiresistive gas sensing. The induced magnetic moment was also investigated for all cases, and only NO adsorption was found to induce a magnetic moment of 1.02  $\mu_{\text{B}}$ . Hence, apart from chemiresistive sensing, GaAs monolayer could also be used in magnetic sensors for selective detection of NO molecules. Optical reflectivity analysis shows that adsorption of NO and NO<sub>2</sub> increases the reflectivity of GaAs monolayer by 400% and 300%, respectively suggesting possible use in optical gas sensors. In summary, our results indicate that GaAs monolayer holds good prospects as chemiresistive, magnetic and optical sensors for sensitive and selective detection of NO with rapid recovery time.

## Data availability

Source data are available from the corresponding author upon request.

## Conflicts of interest

There are no conflicts of interest to declare.

## Acknowledgements

We acknowledge the computational resources of the Department of Electrical and Electronic Engineering, Bangladesh University of Engineering and Technology.

## Notes and references

- V. Salimian Rizi, F. Sharifianjazi, H. Jafarikhorami, N. Parvin, L. Saei Fard, M. Irani and A. Esmaeilkhani, *Mater. Res. Express*, 2019, **6**, 1150g2.
- W. Yuan and G. Shi, *J. Mater. Chem. A*, 2013, **1**, 10078–10091.
- W. Tian, X. Liu and W. Yu, *Appl. Sci.*, 2018, **8**, 1118.
- J. Cao, Q. Chen, X. Wang, Q. Zhang, H.-D. Yu, X. Huang and W. Huang, *Research*, 2021, **2021**, 1–38.
- M. R. Masuk, M. F. Hossain and J. Mahadi, *IEEE Int. Conf. Telecommun. Photonics, Dhaka, Bangladesh*, 2021, 1–4.
- K. Khaliji, S. R. Biswas, H. Hu, X. Yang, Q. Dai, S. H. Oh, P. Avouris and T. Low, *Phys. Rev. Appl.*, 2020, **13**, 1–6.
- M. D. Pedowitz, S. Kim, D. I. Lewis, B. Uppalapati, D. Khan, F. Bayram, G. Koley and K. M. Daniels, *J. Microelectromech. Syst.*, 2020, **29**, 846–852.
- A. Salehi-Khojin, D. Estrada, K. Y. Lin, M. H. Bae, F. Xiong, E. Pop and R. I. Masel, *Adv. Mater.*, 2012, **24**, 53–57.
- Y. Lei, D. Butler, M. C. Lucking, F. Zhang, T. Xia, K. Fujisawa, T. Granzier-Nakajima, R. Cruz-Silva, M. Endo, H. Terrones, M. Terrones and A. Ebrahimi, *Sci. Adv.*, 2020, **6**, 1–10.
- D. Zhao, X. Fan, Z. Luo, Y. An and Y. Hu, *Phys. Lett. A*, 2018, **382**, 2965–2973.
- G. Lu, S. Park, K. Yu, R. S. Ruoff, L. E. Ocola, D. Rosenmann and J. Chen, *ACS Nano*, 2011, **5**, 1154–1164.
- W. Yuan and G. Shi, *J. Mater. Chem. A*, 2013, **1**, 10078–10091.
- C. Yi, W. Wang and C. Shen, *AIP Adv.*, 2014, **4**, 031330.
- F. Schedin, A. K. Geim, S. V. Morozov, E. W. Hill, P. Blake, M. I. Katsnelson and K. S. Novoselov, *Nat. Mater.*, 2007, **6**, 652–655.
- A. Zhang, H. Yang, Q. Liu, W. Li and Y. Wang, *Synth. Met.*, 2020, **266**, 116441.
- T. Wang, R. Zhao, M. Zhao, X. Zhao, Y. An, X. Dai and C. Xia, *J. Mater. Sci.*, 2017, **52**, 5083–5096.
- Q. Yue, Z. Shao, S. Chang and J. Li, *Nanoscale Res. Lett.*, 2013, **8**, 1–7.
- Z. Zhao, Y. Yong, Q. Zhou, Y. Kuang and X. Li, *ACS Omega*, 2020, **5**, 12364–12373.
- S. Ma, D. Yuan, Y. Wang and Z. Jiao, *J. Mater. Chem. C*, 2018, **6**, 8082–8091.
- Y. Yong, X. Su, H. Cui, Q. Zhou, Y. Kuang and X. Li, *ACS Omega*, 2017, **2**, 8888–8895.



- 21 Adsorption of gas molecules on graphene-like InN monolayer: a first-principle study – ScienceDirect, <https://www.sciencedirect.com/science/article/abs/pii/S0169433217302878>, accessed 17 February 2021.
- 22 G. Wang, J. Yu, K. Zheng, Y. Huang, X. Li, X. Chen and L. Q. Tao, *IEEE Electron Device Lett.*, 2020, **41**, 1404–1407.
- 23 S. Ma, D. Li, X. Rao, X. Xia, Y. Su and Y. Lu, *Adsorption*, 2020, **26**, 619–626.
- 24 L. Lin, T. Liu, Y. Zhang, R. Sun, W. Zeng and Z. Wang, *Ceram. Int.*, 2016, **42**, 971–975.
- 25 C. Feng, H. Qin, D. Yang and G. Zhang, *Materials*, 2019, **12**, 676.
- 26 J. Ren, W. Kong and J. Ni, *Nanoscale Res. Lett.*, 2019, **14**, 133.
- 27 X. Sun, Q. Yang, R. Meng, C. Tan, Q. Liang, J. Jiang, H. Ye and X. Chen, *Appl. Surf. Sci.*, 2017, **404**, 291–299.
- 28 Y. Rouzhahong, M. Wushuer, M. Mamat, Q. Wang and Q. Wang, *Sci. Rep.*, 2020, **10**, 9597.
- 29 B. P. Bahuguna, L. K. Saini, B. Tiwari and R. O. Sharma, *RSC Adv.*, 2016, **6**, 52920–52924.
- 30 J. Wu, Y. Yang, H. Gao, Y. Qi, J. Zhang, Z. Qiao and W. Ren, *AIP Adv.*, 2017, **7**, 035218.
- 31 S. S. Guo, X. M. Wei, J. M. Zhang, G. Q. Zhu and W. J. Guo, *Phys. E*, 2016, **83**, 365–371.
- 32 S. Geravandi, G. Goudarzi, M. J. Mohammadi, S. S. Taghavi-rad and S. Salmanzadeh, *Heal. Scope*, 2015, **4**(2), e24318.
- 33 M. Nitschke, B. J. Smith, L. S. Pilotto, D. L. Pisaniello, M. J. Abramson and R. E. Ruffin, *Int. J. Environ. Health Res.*, 2010, **9**, 39–53.
- 34 J. M. Díaz Cónsul, D. Thiele, R. C. Veses, I. M. Baibich and R. M. Dallago, *Quim. Nova*, 2004, **27**, 432–440.
- 35 A. C. G. César, J. A. Carvalho and L. F. C. Nascimento, *Braz. J. Med. Biol. Res.*, 2015, **48**, 1130–1135.
- 36 J. Kulp, *Regulation*, 1990, **13**, 41–50.
- 37 W. Yu, R. Ramanathan and P. Nath, *Technological Forecasting and Social Change*, 2017, vol. 117(C), pp. 160–169.
- 38 N. Brautbar, M. P. Wu and E. D. Richter, *Arch. Environ. Health*, 2010, **58**, 592–596.
- 39 M. P. Diana, W. S. Roekmijati and W. U. Suyud, *E3S Web Conf.*, 2018, **73**, 06003.
- 40 K. Sircar, J. Clower, M. K. Shin, C. Bailey, M. King and F. Yip, *Am. J. Emerg. Med.*, 2015, **33**, 1140–1145.
- 41 F. Li, H. C. O. Chan, S. Liu, H. Jia, H. Li, Y. Hu, Z. Wang and W. Huang, *Forensic Sci. Int.*, 2015, **253**, 112–118.
- 42 Y. Yong, C. Li, X. Li, T. Li, H. Cui and S. Lv, *J. Phys. Chem. C*, 2015, **119**, 7534–7540.
- 43 The Merck Index Online, <https://www.nj.gov/health/eoh/rtkweb/documents/fs/1010.pdf> (accessed December 2021).
- 44 H. Steinebach, S. Kannan, L. Rieth and F. Solzbacher, *Sens. Actuators, B*, 2010, **151**, 162–168.
- 45 I. Hotovy, J. Huran, P. Siciliano, S. Capone, L. Spiess and V. Rehacek, *Sens. Actuators, B*, 2004, **103**, 300–311.
- 46 K. Anand, O. Singh, M. P. Singh, J. Kaur and R. C. Singh, *Sens. Actuators, B*, 2014, **195**, 409–415.
- 47 J. Ni, J. Chang, T. Liu, Y. Li, Y. Zhao and Q. Wang, *Asia-Pacific Optical Fiber Sensors Conference*, 2008, pp. 5–8.
- 48 B. Delley, *J. Chem. Phys.*, 2000, **113**, 7756–7764.
- 49 S. J. Clark, M. D. Segall, C. J. Pickard, P. J. Hasnip, M. I. J. Probert, K. Refson and M. C. Payne, *Z. Kristallog.*, 2005, **220**, 567–570.
- 50 I. Rozahun, T. Bahti, G. He, Y. Ghupur, A. Ablat and M. Mamat, *Appl. Surf. Sci.*, 2018, **441**, 401–407.
- 51 A. Albar and S. A. Aravindh, *J. Phys. Condens. Matter*, 2021, **33**, 475701.
- 52 H. V. Thang, T. L. M. Pham and G. Pacchioni, *Surf. Sci.*, 2022, **716**, 121978.
- 53 Y. Hwang and Y. C. Chung, *Appl. Surf. Sci.*, 2014, **299**, 29–34.
- 54 M. A. Islam, H. Li, S. Moon, S. S. Han, H. S. Chung, J. Ma, C. Yoo, T. J. Ko, K. H. Oh, Y. Jung and Y. Jung, *ACS Appl. Mater. Interfaces*, 2020, **12**, 53174–53183.
- 55 A. Ghojavand, S. J. Hashemifar, M. Tarighi Ahmadpour, A. V. Shapeev, A. Alhaji and Q. Hassanzada, *J. Appl. Phys.*, 2020, **127**, 214301.
- 56 S. Zhu and S. Ma, *Appl. Sci.*, 2019, **9**, 3390.
- 57 Y. Rouzhahong, M. Wushuer, M. Mamat, Q. Wang and Q. Wang, *Sci. Rep.*, 2020, **10**, 1–7.
- 58 H. Guo, W. Zhang, N. Lu, Z. Zhuo, X. C. Zeng, X. Wu and J. Yang, *J. Phys. Chem. C*, 2015, **119**, 6912–6917.
- 59 Y. Wang, N. Song, X. Song, T. Zhang, D. Yang and M. Li, *Vacuum*, 2018, **147**, 18–23.
- 60 X. F. Yu, Y. C. Li, J. B. Cheng, Z. B. Liu, Q. Z. Li, W. Z. Li, X. Yang and B. Xiao, *ACS Appl. Mater. Interfaces*, 2015, **7**, 13707–13713.
- 61 M. Qazi, G. Koley, S. Park and T. Vogt, *Appl. Phys. Lett.*, 2007, **91**, 043113.
- 62 J. H. Li, J. Wu and Y. X. Yu, *Appl. Surf. Sci.*, 2021, **546**, 149104.
- 63 S. S. Abed Al-Abbas, M. K. Muhsin and H. R. Jappor, *Superlattices Microstruct.*, 2019, **135**, 106245.
- 64 A. Aboali and F. Safari, *J. Comput. Electron.*, 2020, **19**, 1373–1379.
- 65 H. Nazemi, A. Joseph, J. Park and A. Emadi, *Sensors*, 2019, **19**, 1285.
- 66 T. Liu, Z. Cui, X. Li, H. Cui and Y. Liu, *ACS Omega*, 2021, **6**, 988–995.
- 67 S. Ma, D. Yuan, Z. Jiao, T. Wang and X. Dai, *J. Phys. Chem. C*, 2017, **121**, 24077–24084.
- 68 R. Bogue, *Sens. Rev.*, 2015, **35**, 133–140.
- 69 J. Wu, G. Yue, W. Chen, Z. Xing, J. Wang, W. R. Wong, Z. Cheng, S. Y. Set, G. Senthil Murugan, X. Wang and T. Liu, *ACS Photonics*, 2020, **7**, 2923–2940.
- 70 R. S. El Shamy, D. Khalil and M. A. Swillam, *Sci. Rep.*, 2020, **10**, 1–9.
- 71 P. V. Shinde and C. S. Rout, *Nanoscale Adv.*, 2021, **3**, 1551–1568.
- 72 D. Ma, Y. Su, T. Tian, H. Yin, C. Zou, T. Huo, N. Hu, Z. Yang and Y. Zhang, *ACS Appl. Mater. Interfaces*, 2020, **12**, 37418–37426.
- 73 D. Matatagui, O. V. Kolokoltsev, N. Qureshi, E. V. Mejía-Uriarte and J. M. Saniger, *Nanoscale*, 2015, **7**, 9607–9613.
- 74 T. Xie, P. Wang, C. Tian, G. Zhao, J. Jia, C. Zhao and H. Wu, *Appl. Phys. Lett.*, 2021, **119**, 013104.
- 75 X. Fu, S. Jiao, N. Dong, G. Lian, T. Zhao, S. Lv, Q. Wang and D. Cui, *RSC Adv.*, 2018, **8**, 390–395.



- 76 S. Peng, K. Cho, P. Qi and H. Dai, *Chem. Phys. Lett.*, 2004, **387**, 271–276.
- 77 Z. Mao, S. Dong, J. Li, X. Lin, X. Jian and P. Wu, *Appl. Surf. Sci.*, 2021, **536**, 147759.
- 78 Y. Yong, H. Cui, Q. Zhou, X. Su, Y. Kuang and X. Li, *RSC Adv.*, 2017, **7**, 51027–51035.
- 79 S. M. Aghaei, M. M. Monshi, I. Torres and I. Calizo, *Appl. Surf. Sci.*, 2018, **427**, 326–333.
- 80 W. Pan, N. Qi, B. Zhao, S. Chang and S. Ye, *Phys. Chem. Chem. Phys.*, 2019, **21**, 11455–11463.
- 81 M. A. Abdulsattar, R. H. Jabbar and H. H. Abed, *J. Phys.: Conf. Ser.*, 2021, **1963**, 012033.
- 82 A. Abbasi and J. J. Sardroodi, *Environ. Sci. Nano*, 2016, **3**, 1153–1164.

